



**HAL**  
open science

## THE N-TERMINAL DOMAIN OF ANNEXIN 2 SERVES AS A SECONDARY BINDING SITE DURING MEMBRANE BRIDGING

Malik Zibouche, Michel Vincent, Françoise Illien, Jacques Gallay, Jesus  
Ayala-Sanmartin

► **To cite this version:**

Malik Zibouche, Michel Vincent, Françoise Illien, Jacques Gallay, Jesus Ayala-Sanmartin. THE N-TERMINAL DOMAIN OF ANNEXIN 2 SERVES AS A SECONDARY BINDING SITE DURING MEMBRANE BRIDGING. *Journal of Biological Chemistry*, 2008, 283 (32), pp.22121-7. 10.1074/jbc.M801000200 . hal-02512403

**HAL Id: hal-02512403**

**<https://hal.science/hal-02512403>**

Submitted on 19 Mar 2020

**HAL** is a multi-disciplinary open access archive for the deposit and dissemination of scientific research documents, whether they are published or not. The documents may come from teaching and research institutions in France or abroad, or from public or private research centers.

L'archive ouverte pluridisciplinaire **HAL**, est destinée au dépôt et à la diffusion de documents scientifiques de niveau recherche, publiés ou non, émanant des établissements d'enseignement et de recherche français ou étrangers, des laboratoires publics ou privés.

## THE N-TERMINAL DOMAIN OF ANNEXIN 2 SERVES AS A SECONDARY BINDING SITE DURING MEMBRANE BRIDGING

Malik Zibouche<sup>1,2</sup>, Michel Vincent<sup>3,4</sup>, Françoise Illien<sup>1,2</sup>, Jacques Gallay<sup>3,4</sup>, and Jesus Ayala-Sanmartin<sup>1,2</sup>.

From <sup>1</sup>INSERM UMRS893, CdR Saint-Antoine, Paris, F-75012 ; <sup>2</sup>Université Pierre et Marie Curie, CHU Saint-Antoine, Paris, F-75012 ; <sup>3</sup>CNRS UMR8619 IBBMC, Orsay, F-91405; <sup>4</sup>Université Paris-Sud, Orsay, F-91405

Running head: The Annexin A2 N-terminal domain associates with membranes

Address correspondence to: Jesus Ayala-Sanmartin, INSERM UMRS893, CdR Saint Antoine, 27 rue Chaligny, 75012 Paris, France. Tel: 33 1 40 01 13 24. Fax: 33 1 40 01 13 90. E-mail: [jayala@chusa.jussieu.fr](mailto:jayala@chusa.jussieu.fr), and Jacques Gallay, IBBMC, UMR8619 CNRS Université Paris-Sud Bâtiment 430, F-91405 Orsay. Tel.: 33 1 69 15 48 42; fax: 33 1 69 85 37 15; e-mail: [jacques.gallay@u-psud.fr](mailto:jacques.gallay@u-psud.fr)

**Annexin A2 (AnxA2) is a Ca<sup>2+</sup>- and acidic phospholipid-binding protein involved in many cellular processes. It undergoes Ca<sup>2+</sup>-mediated membrane bridging at neutral pH and has been demonstrated to be involved in an H<sup>+</sup>-mediated mechanism leading to a novel AnxA2-membrane complex structure. We used fluorescence techniques to characterize this H<sup>+</sup>-dependent mechanism at the molecular level, in particular the involvement of the AnxA2 N-terminal domain. This domain was labeled at Cys8 either with acrylodan or pyrene-maleimide fluorescent probes. Steady-state and time-resolved fluorescence analysis for acrylodan and fluorescence quenching by doxyl-labelled phospholipids revealed direct interaction between the N-terminal domain and the membrane. The absence of pyrene excimer suggested that interactions between N-termini are not involved in the H<sup>+</sup>-mediated mechanism. These findings differ from those previously observed for the Ca<sup>2+</sup>-mediated mechanism. Protein titration experiments showed that the protein concentration for half-maximal membrane aggregation was twice for Ca<sup>2+</sup>-mediated compared to H<sup>+</sup>-mediated aggregation, suggesting that AnxA2 was able to bridge membranes either as a dimer or as a monomer, respectively. A N-terminally deleted AnxA2 was two to three times less efficient than the wild type protein for H<sup>+</sup>-mediated membrane aggregation. We propose a model of AnxA2-membrane assemblies, highlighting the different roles of the N-terminal domain in the H<sup>+</sup>- and Ca<sup>2+</sup>-mediated membrane bridging mechanisms.**

(1,2). These proteins have two structural domains: a C-terminal core with a conserved structure and a N-terminal domain variable in sequence and length (3). The core domain is formed by four repeats (or eight for AnxA6) containing Ca<sup>2+</sup> binding sites. Each repeat consists of five  $\alpha$ -helices connected by short loops. The four repeats are organized into a slightly curved oblate shape with a convex face harboring the Ca<sup>2+</sup> binding sites, allowing contact with membrane phospholipids. The variable N-terminal domain, facing the concave surface at the opposite side of the membrane bilayer, contains interaction sites for other protein partners. This domain harbors a number of posttranslational modifications and regulates the membrane-activity properties of the core domain.

Anx proteins not only bind the surface of model and biological membranes but can also assemble into different structures on these surfaces. Some of these proteins including AnxA5 can assemble into lateral structures forming two-dimensional networks on the membrane surface (4-6). Others, including AnxA1 and AnxA2 form membrane junctions with or without protein ligands attached to their N-terminal segment (7-11). The classical mechanism described for these two processes involves a primary Ca<sup>2+</sup>-dependent membrane binding step leading to conformational changes of the core domain, in particular of repeat III (12-18). The N-terminal domain of Anxs also plays an important role in the specific membrane aggregative properties. In particular, the N-terminal domain of AnxA1 and AnxA2 interacts strongly with proteins of the S100 family, resulting in a several-fold increase in the Ca<sup>2+</sup> sensitivity of membrane aggregation (17). Recently, we showed that the N-terminal domain of monomeric AnxA2 was also involved in the Ca<sup>2+</sup>-dependent membrane bridging at neutral

Annexins (Anx) belong to a family of Ca<sup>2+</sup>-dependent phospholipid-binding proteins and have various membrane-related functions

pH: we demonstrated interactions between the N-terminal domains of two adjacent AnxA2 molecules, which were not in direct contact with the membrane phospholipids (19).

Besides this classical  $\text{Ca}^{2+}$ -dependent mechanism, Anx proteins also bind both model and cellular membranes independently of calcium ions (20,21) or in a proton-dependent manner (22-27). This  $\text{Ca}^{2+}$ -independent binding is associated with an increased hydrophobicity of Anx at acidic pH (28,29), and may involve a significant conformational change of the core generating a transmembrane form of the protein as suggested for AnxB12 (23,30). This hypothesis has been extended to AnxA5 (24) and AnxA6 (25), but not for AnxA1 and A2. AnxA2 undergoes an  $\text{H}^+$ -dependent conformational change of repeat III, very similar to that in the presence of  $\text{Ca}^{2+}$  at neutral pH, but the  $\text{H}^+$ -mediated binding at the membrane surface did not involve further structural modification of the core domain (17). The monomeric AnxA2 started to form bridges in vitro in the absence of  $\text{Ca}^{2+}$  at pH 6 and attained the maximal bridging at pH 5.2. However, the organization of the membrane junctions at acidic pH differed from that at neutral pH (26).

We investigated the molecular structure of these novel membrane junctions previously observed by cryo-electron microscopy (26) for monomeric AnxA2 at pH 4. In particular we studied the dynamics of the N-terminal domain in the free soluble form of the protein at acidic pH in the absence of calcium and the conformational and environment changes of this domain that may occur during membrane bridging, using steady-state and time-resolved fluorescence techniques. We specifically labeled the reactive cysteine Cys8 in the N-terminus by thiol-reactive fluorescent markers (19,31). We used 6-acryloyl-2-dimethylaminonaphthalene (acrylodan), a polarity-sensitive probe (32,33) to detect environment and mobility changes of the N-terminal domain and the excimer-sensitive probe N-(1-pyrene)maleimide (pyrene-maleimide) (34), to detect potential interactions between N-termini that we previously showed for the  $\text{Ca}^{2+}$ -dependent membrane bridging mechanism at neutral pH (19). We propose a model, based on our findings, for the organization of AnxA2 in  $\text{Ca}^{2+}$ - and  $\text{H}^+$ -mediated membrane bridging.

## Experimental Procedures

*Chemicals-* Acrylodan and N-(1-pyrene)maleimide were purchased from Molecular Probes (Invitrogen, France). Type III-B egg L- $\alpha$ -phosphatidylcholine (PC) and brain L- $\alpha$ -phosphatidyl-L-serine (PS) were obtained from Sigma-Aldrich, France. Dr. Claude Wolf (CHU Saint-Antoine, Paris) kindly provided 1-palmitoyl-2-stearoyl(n-doxyl)-sn-glycerophosphatidylcholine (n-doxyl PC) derivatives labelled with a doxyl group at positions n = 5, 7 and 12 of the sn2 chain.

*Protein preparation and labelling with acrylodan and pyrene maleimide-* AnxA2 produced in *S. cerevisiae* was purified as previously described (35). Protein purity was estimated as >95% by gel electrophoresis. The N-terminally deleted AnxA2 ( $\Delta\text{N}$ -AnxA2) was prepared as described in (10). The only reactive cysteine of AnxA2, Cys8, was labelled with acrylodan or pyrene maleimide using the method of Johnsson *et al.* (31) previously described in (19). The efficiency of acrylodan labelling was 50% and that of pyrene-maleimide labelling was 83% (see (19)). Labelled proteins were stored at  $-20^\circ\text{C}$ . Membrane aggregative properties did not appear to differ between labelled and unlabelled proteins.

*LUV preparation and aggregation-* Large unilamellar vesicles (LUV) (PC/PS: 75/25 weight ratio) were prepared by extrusion as previously described (36). Briefly, lipids were mixed together in chloroform. The solvent was removed from the mixture under a stream of nitrogen. Residual solvent was removed under vacuum for one hour. Lipids were then resuspended in buffer A (40 mM Hepes pH 7, 30 mM KCl, 1 mM EGTA) at a final concentration of  $1 \text{ mg ml}^{-1}$ , by vortexing vigorously. The multilamellar liposomes were then extruded by passing the suspension 21 times through a polycarbonate membrane with  $0.1 \mu\text{m}$  pores (Avestin, Canada). Free calcium concentration, expressed as pCa ( $-\log [\text{Ca}^{2+}]$ ), was controlled by EGTA buffering. Vesicle aggregation was monitored in buffer A in the presence of calcium, or in buffer B (40 mM Acetate pH 4, 30 mM KCl, 1mM EGTA) for pH 4 experiments, by turbidimetry at 340 nm, as previously described (37).

*Steady-state fluorescence measurements-* Fluorescence emission spectra were recorded with a Cary Eclipse spectrofluorimeter with slit width of 10 nm and 5 nm for excitation and emission, respectively. Samples were contained in microcuvettes (120  $\mu\text{l}$ ).

### *Time-resolved fluorescence measurements*

Fluorescence intensity and anisotropy decays were obtained from the polarized  $I_{vv}(t)$  and  $I_{vh}(t)$  components measured by the time-correlated single-photon counting technique. A diode laser (LDH 405 from Picoquant, Berlin-Adlershof, Germany; maximal emission at 392 nm) operating at 10 MHz was used as an excitation source. A Hamamatsu fast photomultiplier (model R3235-01) was used for detection. Emission wavelength was selected with a Jobin-Yvon H10 monochromator (band width 16 nm) and a Schott KV418 cut-off filter. Each experimental decay  $I_{vv}(t)$  and  $I_{vh}(t)$  was stored on a 2 K plug-in multichannel analyzer card (Ortec Trump-PCI 2k, Ametek France), using Maestro-32 software. Automatic data sampling was controlled by the microcomputer. The instrumental response function (FWHM ~600 ps) was collected automatically by measuring the light scattering of a glycogen solution during 30 s at the excitation wavelength, alternating with the parallel and perpendicular components of polarized fluorescence decay, each over a total of 90 s. Samples were contained in microcuvettes (120  $\mu$ l).

Fluorescence intensity decay analyses were performed with maximum entropy method (MEM), using a multiexponential model,  $\sum_i \alpha_i \exp(-t/\tau_i)$ , as previously described (38). A classical anisotropy model,  $\sum_i \beta_i \exp(-t/\theta_i)$ , in which any rotational correlation time ( $\theta$ ) is coupled with each lifetime ( $\tau$ ), was used to resolve polarized fluorescence decays (39). Calculations were carried out with a set of 150 or 100 independent variables (equally spaced on a logarithmic scale) for intensity and anisotropy, respectively. The programs, including the MEMSYS 5 subroutines (MEDC Ltd, Cambridge, UK), were written in double-precision FORTRAN 77.

*Fluorescence quenching by doxyl-PCs*  
Quenching by doxyl-PCs (distearoylphosphatidylcholine (PC) labelled with a doxyl group bound at C5, C7 and C12 on the sn2 acyl chain) was carried out with LUV prepared with 10, 20 or 30% molar fractions of labelled PC, 25% PS and supplemented with unlabelled PC. The distance,  $Z_{cf}$ , from the centre of the bilayer can be estimated according to the expression:

$$Z_{cf} = \frac{1}{-\pi \times C} \times \ln \frac{F_1}{F_2} - L_{21}^2 + L_{c1},$$

where  $F_1$  and  $F_2$  are the fluorescence intensities of the fluorophore in the presence of the shallow and of the deeper quenchers, respectively;  $L_{21}$  is the vertical distance between the shallow and the deep quenchers;  $L_{c1}$  is the distance between the shallow quencher and the centre of the bilayer; and  $C$  is the concentration of the quenchers in molecules per unit area (40). The distance of the quenchers from the centre of the bilayer was 12.15 Å for 5-doxyl PC and 5.85 Å for 12-doxyl PC (41).

## RESULTS

*Conformational dynamics of the acrylodan-labelled AnxA2 N-terminal segment in solution at pH 4.* The steady-state fluorescence emission spectrum of Annexin A2 labelled with acrylodan (AnxA2<sup>acryl</sup>) at pH 4 peaked at 515-520 nm, consistent with previously reported values at neutral pH. Thus, the environment of acrylodan bound to Cys8 in the N-terminal segment remained highly polar in mild acidic conditions (Fig. 1). The fluorescence intensity decay was not monoexponential (Fig. 2A). MEM analysis of the data showed the presence of three lifetime populations (Fig. 2B & C), probably attributable to the existence of three local conformers: we did not detect any sign of excited-state reaction, such as fluorescence build-up at long emission wavelength (data not shown). The centre value and amplitude of each lifetime peak are presented in Table 1. The lifetime values are similar to those measured at neutral pH, showing that mild acidification does not alter the interactions between acrylodan and its microenvironment. However, we observed an H<sup>+</sup>-induced redistribution of the long and the intermediate lifetime amplitudes, involving a significant increase of the amplitude average lifetime by ~15%: thus, mild acidification seemed to induce a redistribution of local conformers.

Fluorescence anisotropy decay of AnxA2<sup>acryl</sup> showed rapid dynamics of the AnxA2 N-terminal segment at pH 4, consistent with that observed at neutral pH. The experimental anisotropy decay curve decreased rapidly at first, and then more slowly (Fig. 3). Two time constants were calculated: a subnanosecond component and a much longer component (Table

2). The short decay time probably reflects the local, partially restricted motion of acrylodan around its linker. The semi-angle value of the wobbling-in-cone subnanosecond rotation  $\omega_{max}$  was large. The longest rotational correlation time value probably corresponds to the Brownian rotational motion of the protein. This value is significantly smaller at pH 4 than at pH 7 (19), consistent with the more compact state of the protein at mild acidic pH in solution (26).

*Conformational dynamics of the acrylodan-labelled AnxA2 N-terminal segment upon membrane bridging at pH 4.* Interaction of AnxA2<sup>acryl</sup> with negative phospholipid membranes at mild acidic pH, shifted the fluorescence emission spectrum of acrylodan to shorter wavelengths (from 515 nm to 470 nm for L/P=100) (Fig. 1). The amplitude of the shift (45 nm) is significantly larger than that observed at pH 7 in the presence of calcium (30 nm) (19), suggesting that the microenvironment of acrylodan is more apolar when the protein interacts with the membrane in mild acidic conditions than at neutral pH in the presence of calcium. The fluorescence intensity decay changed slightly upon membrane bridging (Fig. 2 & Table 1), indicating a local conformational change of the N-terminal segment during these processes.

The AnxA2-induced membrane bridging caused a significant decrease of the local dynamics of the N-terminal segment compared to the protein in solution, as shown by fluorescence anisotropy decay (Fig. 3). MEM analysis computed two rotational correlation time populations (Table 2). A nanosecond rotational motion appeared and the longest rotational correlation time value increased substantially. However, the initial anisotropy value  $A_{t=0}$  was significantly lower than the intrinsic anisotropy value in vitrified media (42), thus subnanosecond rotation was probably present. The semi-angle of the acrylodan subnanosecond wobbling-in-cone rotation  $\omega_{max}$  also decreased considerably (Table 2), confirming a much larger restriction of movement than that previously observed for the Ca<sup>2+</sup>-dependent membrane bridging mechanism at neutral pH (19).

*Location of the AnxA2 N-terminal segment in bridged membranes in mild acidic conditions.* We showed above that when monomeric AnxA2<sup>acryl</sup> binds to LUV in mild acidic conditions, favouring membrane aggregation, the

fluorophore moved to a hydrophobic environment. Direct interactions of the N-terminus with the membrane, as previously described for AnxA1 (22,43-45) may underlie these observations. To determine the extent of AnxA2<sup>acryl</sup>-membrane interactions, quenching experiments were performed with LUV (PC/PS 75/25) containing *n*-doxyl PC at different mole fractions (10, 20 and 30) (40,46). The various *n*-doxyl PCs showed high levels of quenching efficiency (up to 80%), depending on their mole fractions (Fig. 4). These findings demonstrated that acrylodan bound to Cys8 on the N-terminal segment of the protein interacted strongly with the membrane lipids. The distance of the acrylodan moiety from the centre of the bilayer was estimated from the quenching efficiency values of the shallow 5-doxyl PC and that of the deeper 12-doxyl PC derivatives to be 10.7 Å.

Ca<sup>2+</sup>-induced membrane bridging by monomeric AnxA2 at neutral pH involves interactions between their N-terminal segments, previously demonstrated by disulfide bond formation (47), and by the formation of excimers using AnxA2 labelled by N-pyrene maleimide on Cys8 (19). However, in the absence of calcium and at pH 4, we did not observe the spectral signature corresponding to excimer formation (emission peak at 455 nm) (34). for the AnxA2-membrane complex, suggesting that N-terminal domain dimerisation is not required for membrane bridging in mild acidic conditions (Fig. 5).

*Molecular organisation of AnxA2 in membrane bridges in mild acidic pH.* In membrane bridging experiments, the rise in turbidity (vesicles aggregation) was greater at pH 4 in the absence of calcium than at pH 7 in its presence. We previously viewed membrane bridges by cryo-electron microscopy in mild acidic conditions and found that monomeric AnxA2 was mainly organized in a single protein layer (26), whereas at pH 7, in the presence of calcium mainly two protein layers were observed, indicating 'face-to-face' dimerization of AnxA2 molecules (11). Thus, two molecules appeared to be necessary for membrane bridging in the presence of calcium at neutral pH, but only one molecule was required at mild acidic pH. It would thereby follow that protein concentration needed to attain half maximal extent of aggregation at pH 4 must be two-fold lower than that at pH 7 in the presence of calcium. To test this hypothesis, the extent of aggregation was measured as a function of protein concentration. Indeed, the protein

concentration giving half maximal aggregation at pH 4 was  $2.5 \pm 0.2 \mu\text{g ml}^{-1}$  and  $5.1 \pm 0.2 \mu\text{g ml}^{-1}$  at pH 7 in the presence of calcium (pCa 3) (Fig. 6A). The magnitude of cooperativity of  $\text{Ca}^{2+}$ -induced membrane aggregation at pCa 3 (two molecules) was greater (Hill number 0.90) than at pH 4 (one molecule) (Hill number 0.34).

The protein titration experiments suggested that at acidic pH, membrane bridging required only one molecule of AnxA2, and the quenching experiments by n-doxyl PC that the N-terminal domain was in contact with the membrane. To test the role of the N-terminal domain contact with the membrane in bridging, we compared the abilities of the complete and the N-terminally deleted AnxA2 ( $\Delta\text{N-AnxA2}$ ) abilities for membrane aggregation. As shown in Fig. 6B,  $\Delta\text{N-AnxA2}$  is able to bridge membranes, but the extent of aggregation is two to three-fold lower than the aggregation mediated by the complete protein. This indicates that the contact of the N-terminal domain with the membrane is not strictly necessary but is important to enhance the capacity of the protein to form membrane bridges at acidic pH.

## DISCUSSION

The annexin family of membrane binding proteins binds negatively charged phospholipid membranes through either  $\text{Ca}^{2+}$ -dependent or  $\text{Ca}^{2+}$ -independent/ $\text{H}^+$ -dependent mechanisms (20,24,26,29). The classical  $\text{Ca}^{2+}$ -dependent binding and aggregation mechanisms have been extensively studied (see (2) for a review). Several aspects of the  $\text{H}^+$ -dependent binding have been studied for annexins A1, A2, A5, A6, and B12. Two types of membrane interaction have been proposed: insertion of the protein into the membrane bilayer, resulting in a transmembrane form of the protein (in particular AnxB12 (30,48,49)), and the association at the membrane surface without large structural changes of the core domain (shown for AnxA2 (26)). A modulatory role of the AnxA1 N-terminal domain in  $\text{H}^+$ -mediated binding has also been suggested (22).

In this study, we investigated the dynamics of the AnxA2 N-terminal domain and its localization with respect to the membrane during the  $\text{H}^+$ -mediated membrane bridging. We previously demonstrated that AnxA2 aggregated membranes in the pH range (6-5.2) (26), a pH range in agreement with that published for AnxA2 in cells (50). The experiments in this study were

performed at pH 4 to avoid data misinterpretation due to mixed AnxA2 populations (soluble, bound and aggregative forms), and to favor 100% of the protein in membrane bridges. The N-terminal domain was labeled on Cys8 by thiol-specific fluorescent probes: acrylodan and pyrene-maleimide. The characteristics of the N-terminal domain during  $\text{H}^+$ -mediated membrane bridging were compared with those previously observed for the  $\text{Ca}^{2+}$ -mediated processes.

In solution, the N-terminal tail of AnxA2 at pH 4 was as flexible as at pH 7 with  $\text{Ca}^{2+}$ . We did not detect any  $\text{H}^+$ -induced conformational change of this domain similarly to our previous observations with  $\text{Ca}^{2+}$  (19). This is in contrast to the core domain, where we observed a  $\text{H}^+$ - (26) and a  $\text{Ca}^{2+}$ -induced restricted mobility (17) for the sole tryptophan residue (W212) in repeat III. The two domains of the AnxA2 molecule behave therefore independently.

The environment and dynamics of acrylodan bound to the N-terminal domain of the protein in  $\text{H}^+$ -induced membrane bridges differed from those previously observed in  $\text{Ca}^{2+}$ -induced membrane bridges: the environment was less polar and the subnanosecond mobility more restricted than in the  $\text{Ca}^{2+}$ -induced membrane-bridged state. Furthermore, the n-doxyl PC quenchers also behaved differently in the two conditions: in the  $\text{H}^+$ -driven membrane-bridged mechanism, highly efficient quenching revealed strong interactions between the N-terminal domain and the membrane, whereas a low level of quenching in the  $\text{Ca}^{2+}$ -induced state indicated the absence of these strong interactions (19). Additionally, the geometry of the junctions differed in these two conditions: the  $\text{Ca}^{2+}$ -induced mechanism involves interactions between N-termini, demonstrated previously by formation of excimers with N-pyrene-maleimide-labelled monomeric AnxA2 (19), that were not observed in this study, thereby suggesting that such interactions did not occur in the  $\text{H}^+$ -mediated membrane bridging mechanism at mild acidic pH.

The distribution of protein charges can provide information about the topology of the  $\text{H}^+$ -dependent membrane junctions. Anx A2 is mainly neutral with a theoretical isoelectric point of 7.56 but the distribution of the charged residues is not homogeneous. The core exhibits strong positively charged regions on its convex face, with many Lys residues (49 in repeat I; 340, 206 and 249 in repeat III; 279, 281, 313 and 324 in repeat IV) and some Arg residues (205 and

245 in repeat III) exposed at the surface. These residues can make electrostatic bridges with the negatively charged PS headgroups, thereby replacing the  $\text{Ca}^{2+}$  bridges as some of these Lys residues are close to the  $\text{Ca}^{2+}$ -binding loops. The flanking and the convex surfaces of repeat I also have a strong positive charge density, probably favoring interaction between the N-terminal segment and the negatively charged membrane surface. The N-terminal segment (residues 1 to 30) has a net charge of +5 at pH 4. The first 14 residues of this segment are able to behave like an amphipathic  $\alpha$ -helix in different conditions such as in water/TFE mixtures (51), and when complexed with S100A10 (p11) (52). It is thus possible that the N-terminal domain may fold as an amphipathic helix on the membrane surface in a similar way as when complexed with S100A10 (p11). This helix could interact with the membrane surface through salt bridges involving His4 and Lys9. In such conformation, acrylodan bound to Cys8 would be located on the hydrophilic side of the helix (52). Its spectroscopic properties showed however that it should be located inside the membrane bilayer. This potential amphipathic helix could therefore lie at the membrane/water interface, with its hydrophilic side located at a shallow position in this interface, thus acrylodan would then be in contact with the acyl chains, the hydrophobic side of the helix facing the concave face of the protein.

We propose a model incorporating previous findings and those from this study, implicating two mechanisms for the monomeric AnxA2 organization during membrane bridging (Fig. 7): one being  $\text{Ca}^{2+}$ -mediated and the other  $\text{H}^+$ -mediated. In cells, levels of  $\text{H}^+$  and  $\text{Ca}^{2+}$  are interconnected,  $\text{Ca}^{2+}$  gradients being important cofactors of pH-induced effects (50). Our model proposes a balance between these ions that may favor either mode of organization, determined by the physiological conditions and the cellular compartments. Both mechanisms require the presence of acidic phospholipids for interaction of the protein core with the membrane, mediated by either  $\text{Ca}^{2+}$ - or salt bridges. The N-terminal domain appeared to have a different modulating role in each process, probably related with its electrical charge. In the classical  $\text{Ca}^{2+}$ -mediated

mechanism at neutral pH, two N-terminal domains interact, without direct contact with the membrane surface (Fig. 7A) (19). These N-terminal interactions stabilize a complex between two AnxA2 molecules that form the  $\text{Ca}^{2+}$ -mediated membrane bridges, consistent with previous observations by cryo-electron microscopy (11) and with our aggregation experiments in the present study. Our model for  $\text{H}^+$ -dependent membrane bridging, consistent with cryo-electron microscopy studies (26), proposes that these bridges are formed with only one AnxA2 molecule located between two juxtaposed membranes, with the core interacting with one membrane surface on its convex side and the N-terminal domain interacting with the second membrane surface on the concave side, as previously suggested for AnxA1 (22,43) (Fig. 7B). It is possible that some residues on the concave side of the molecule could be involved also in the interactions since the  $\Delta\text{N}$ -AnxA2 was partly able to perform membrane aggregation. Notice that in the presence of calcium and at neutral pH, Lambert et al. (11) observed mainly two protein stripes for AnxA1 and A2, but they also observed some bridges with only one protein stripe. These structures may thus coexist and are not exclusive for one calcium or proton concentration. Other factors such as ionic strength or temperature may be involved in determining the organization of Anx membrane bridges. In both cases, core-core contacts may contribute to the stabilization of the structure as shown by cross linking of AnxA1 (43) and AnxA2 (53). Two possible orientations of the AnxA2 core are schematized. The structure depicted at the bottom of Fig. 7B is consistent with the observation of dimers in the crystal structure of the complete AnxA2 (54).

Finally, the physiological role of the monomeric AnxA2 has been suggested by studies on membrane exocytosis with no S100A10 protein (55) and in particularly acidic organelles (56) such as endosomes in which AnxA2 may have an impact in endosomal membranes fusion. Therefore, the proposed models for AnxA2-mediated membrane bridging are likely to reflect physiological events in cells and this may underlie the calcium-independent membrane binding observed in endosomes (20).

## REFERENCES

1. Rescher, U., and Gerke, V. (2004) *J Cell Sci* **117**, 2631-2639
2. Gerke, V., Creutz, C. E., and Moss, S. E. (2005) *Nat Rev Mol Cell Biol* **6**, 449-461
3. Gerke, V., and Moss, S. E. (2002) *Physiol Rev* **82**, 331-371
4. Mosser, G., Ravanat, C., Freyssinet, J. M., and Brisson, A. (1991) *J Mol Biol* **217**, 241-245
5. Pigault, C., Follenius-Wund, A., Schmutz, M., Freyssinet, J. M., and Brisson, A. (1994) *J Mol Biol* **236**, 199-208
6. Oling, F., Santos, J. S., Govorukhina, N., Mazeret-Dubut, C., Bergsma-Schutter, W., Oostergetel, G., Keegstra, W., Lambert, O., Lewit-Bentley, A., and Brisson, A. (2000) *J Mol Biol* **304**, 561-573.
7. Drust, D. S., and Creutz, C. E. (1988) *Nature* **331**, 88-91
8. Wang, W., and Creutz, C. E. (1994) *Biochemistry* **33**, 275-282
9. Bitto, E., and Cho, W. (1999) *Biochemistry* **38**, 14094-14100
10. Ayala-Sanmartin, J. (2001) *Biochem Biophys Res Commun* **283**, 72-79.
11. Lambert, O., Gerke, V., Bader, M. F., Porte, F., and Brisson, A. (1997) *J Mol Biol* **272**, 42-55
12. Pigault, C., Follenius-Wund, A., Lux, B., and Gerard, D. (1990) *Biochim Biophys Acta* **1037**, 106-114
13. Sopkova, J., Renouard, M., and Lewit-Bentley, A. (1993) *J Mol Biol* **234**, 816-825.
14. Concha, N. O., Head, J. F., Kaetzel, M. A., Dedman, J. R., and Seaton, B. A. (1993) *Science* **261**, 1321-1324.
15. Sopkova, J., Gallay, J., Vincent, M., Pancoska, P., and Lewit-Bentley, A. (1994) *Biochemistry* **33**, 4490-4499
16. Sopkova, J., Vincent, M., Takahashi, M., Lewit-Bentley, A., and Gallay, J. (1999) *Biochemistry* **38**, 5447-5458.
17. Ayala-Sanmartin, J., Vincent, M., Sopkova, J., and Gallay, J. (2000) *Biochemistry* **39**, 15179-15189
18. Sopkova-De Oliveira Santos, J., Vincent, M., Tabaries, S., Chevalier, A., Kerboeuf, D., Russo-Marie, F., Lewit-Bentley, A., and Gallay, J. (2001) *FEBS Lett* **493**, 122-128
19. Ayala-Sanmartin, J., Zibouche, M., Illien, F., Vincent, M., and Gallay, J. (2008) *Biochim Biophys Acta* **1778**, 472-482
20. Jost, M., Zeuschner, D., Seemann, J., Weber, K., and Gerke, V. (1997) *J Cell Sci* **110**, 221-228
21. Ayala-Sanmartin, J., Henry, J., and Pradel, L. (2001) *Biochim Biophys Acta* **1510**, 18-28.
22. Rosengarth, A., Wintergalen, A., Galla, H. J., Hinz, H. J., and Gerke, V. (1998) *FEBS Lett* **438**, 279-284.
23. Langen, R., Iwasaki, J. M., Luecke, H., Haigler, H. T., and Hubbell, W. L. (1998) *J Biol Chem* **273**, 22453-22457
24. Iwasaki, J. M., Cartailier, J. P., Sokolov, Y., Patel, D. R., Langen, R., Luecke, H., Hall, J. E., and Haigler, H. T. (2000) *Biochemistry* **39**, 3015-3022
25. Golczak, M., Kicinska, A., Bandorowicz-Pikula, J., Buchet, R., Szewczyk, A., and Pikula, S. (2001) *Faseb J* **15**, 1083-1085.
26. Lambert, O., Cavusoglu, N., Gallay, J., Vincent, M., Rigaud, J. L., Henry, J. P., and Ayala-Sanmartin, J. (2004) *J Biol Chem* **279**, 10872-10882
27. Monastyrskaya, K., Babiychuk, E. B., Hostettler, A., Rescher, U., and Draeger, A. (2007) *Cell Calcium* **41**, 207-219

28. Genge, B. R., Wu, L. N., Adkisson, H. D. t., and Wuthier, R. E. (1991) *J Biol Chem* **266**, 10678-10685
29. Kohler, G., Hering, U., Zschornig, O., and Arnold, K. (1997) *Biochemistry* **36**, 8189-8194.
30. Kim, Y. E., Isas, J. M., Haigler, H. T., and Langen, R. (2005) *J Biol Chem* **280**, 32398-32404
31. Johnsson, N., Marriott, G., and Weber, K. (1988) *Embo J* **7**, 2435-2442
32. Weber, G., and Farris, F. J. (1979) *Biochemistry* **18**, 3075-3078
33. Prendergast, F. G., Meyer, M., Carlson, G. L., Iida, S., and Potter, J. D. (1983) *J Biol Chem* **258**, 7541-7544
34. Galla, H. J., and Hartmann, W. (1980) *Chem Phys Lipids* **27**, 199-219
35. Ayala-Sanmartin, J., Gouache, P., and Henry, J. P. (2000) *Biochemistry* **39**, 15190-15198
36. Lamaziere, A., Burlina, F., Wolf, C., Chassaing, G., Trugnan, G., and Ayala-Sanmartin, J. (2007) *PLoS ONE* **2**, e201
37. Lamaziere, A., Wolf, C., Lambert, O., Chassaing, G., Trugnan, G., and Ayala-Sanmartin, J. (2008) *PLoS ONE* **3**, e1938
38. Vincent, M., Brochon, J. C., Merola, F., Jordi, W., and Gallay, J. (1988) *Biochemistry* **27**, 8752-8761.
39. Vincent, M., and Gallay, J. (1991) *Eur Biophys J* **20**, 183-191
40. Chattopadhyay, A., and London, E. (1987) *Biochemistry* **26**, 39-45
41. Abrams, F. S., and London, E. (1993) *Biochemistry* **32**, 10826-10831
42. Gallay, J., Vincent, M., Li de la Sierra, I. M., Munier-Lehmann, H., Renouard, M., Sakamoto, H., Barzu, O., and Gilles, A. M. (2004) *Eur J Biochem* **271**, 821-833
43. Bitto, E., Li, M., Tikhonov, A. M., Schlossman, M. L., and Cho, W. (2000) *Biochemistry* **39**, 13469-13477.
44. Rosengarh, A., Gerke, V., and Luecke, H. (2001) *J Mol Biol* **306**, 489-498.
45. Hu, N. J., Bradshaw, J., Lauter, H., Buckingham, J., Solito, E., and Hofmann, A. (2008) *Biophys J* **94**, 1773-1781
46. London, E., and Feigenson, G. W. (1981) *Biochemistry* **20**, 1932-1938
47. Ayala-Sanmartin, J., Cavusoglu, N., Masliah, J., and Trugnan, G. (2004) *Annexins* **1**, 19-25
48. Langen, R., Isas, J. M., Hubbell, W. L., and Haigler, H. T. (1998) *Proc Natl Acad Sci U S A* **95**, 14060-14065
49. Ladokhin, A. S., and Haigler, H. T. (2005) *Biochemistry* **44**, 3402-3409
50. Monastyrskaya, K., Tschumi, F., Babiychuk, E. B., Stroka, D., and Draeger, A. (2008) *Biochem J* **409**, 65-75
51. Hong, Y. H., Won, H. S., Ahn, H. C., and Lee, B. J. (2003) *J Biochem (Tokyo)* **134**, 427-432
52. Rety, S., Sopkova, J., Renouard, M., Osterloh, D., Gerke, V., Tabaries, S., Russo-Marie, F., and Lewit-Bentley, A. (1999) *Nat Struct Biol* **6**, 89-95
53. Faure, A. V., Migne, C., Devilliers, G., and Ayala-Sanmartin, J. (2002) *Exp Cell Res* **276**, 79-89.
54. Rosengarh, A., and Luecke, H. (2004) *Annexins* **1**, 129-136
55. Chasserot-Golaz, S., Vitale, N., Sagot, I., Delouche, B., Dirrig, S., Pradel, L. A., Henry, J. P., Aunis, D., and Bader, M. F. (1996) *J Cell Biol* **133**, 1217-1236
56. Morel, E., and Gruenberg, J. (2007) *PLoS ONE* **2**, e1118

## FOOTNOTES

We would like to thank Dr. C. Wolf for kindly providing the n-doxyl PC derivatives. This work was supported by CNRS and INSERM funding.

The abbreviations used are: Acrylodan, 6-acryloyl-2-dimethylaminonaphthalene; Anx, annexin; AnxA2<sup>acryl</sup>, Annexin A2 labelled with acrylodan on Cys8;  $\Delta$ N-AnxA2, Annexin A2 deleted of the 29 first residues; LUV, large unilamellar vesicles; MEM, maximum entropy method; n-doxyl PC, 1-palmitoyl-2-stearoyl(n-doxyl)-*sn*-glycerophosphatidylcholine (n= 5, 7 or 12); P11, S100A10 protein; PC, egg L- $\alpha$ -glycerophosphatidylcholine; PS brain L- $\alpha$ -glycerophosphatidyl-L-serine; Pyrene-maleimide, N-(1-pyrene)maleimide.

## TABLES

**Table 1**

The effect of AnxA2<sup>acryl</sup> binding to LUV (PC/PS 75/25) at pH 4 on fluorescence intensity decay, measured by MEM of acrylodan. Excitation wavelength: 392 nm; emission wavelength: 510 nm for AnxA2 and 480 nm for AnxA2-LUV. Protein concentration 0.5  $\mu$ M.

Sample	$\tau_1$ (ns) $\alpha_1$	$\tau_2$ (ns) $\alpha_2$	$\tau_3$ (ns) $\alpha_3$	$\langle\tau\rangle$ (ns) <sup>a</sup>
AnxA2	$0.58 \pm 0.11$ $0.22 \pm 0.03$	$1.28 \pm 0.17$ $0.30 \pm 0.06$	$3.37 \pm 0.05$ $0.48 \pm 0.03$	$2.13 \pm 0.03$
AnxA2 LUV L/P=100	$0.17 \pm 0.02$ $0.32 \pm 0.05$	$1.30 \pm 0.09$ $0.22 \pm 0.04$	$3.59 \pm 0.06$ $0.47 \pm 0.06$	$2.01 \pm 0.17$
AnxA2 LUV L/P=150	$0.18 \pm 0.01$ $0.33 \pm 0.01$	$1.32 \pm 0.02$ $0.19 \pm 0.01$	$3.62 \pm 0.06$ $0.48 \pm 0.02$	$2.05 \pm 0.01$

<sup>a</sup> amplitude averaged lifetime :  $\langle \tau \rangle = \sum_i \alpha_i \tau_i$

**Table 2**

The effect of AnxA2<sup>acryl</sup> binding to LUV (PC/PS 75/25) at pH 4 on the fluorescence anisotropy decay of acrylodan; MEM analysis.

Sample	$\theta_1$ (ns)	$\beta_1$	$\theta_2$ (ns)	$\beta_2$	$A_{t=0} = \sum \beta_i$	$\omega_{max}$ (°) <sup>a</sup>
AnxA2	$0.14 \pm 0.03$	$0.191 \pm 0.036$	$15 \pm 2$	$0.232 \pm 0.001$	0.423	$31 \pm 1$
AnxA2 LUV L/P=100	$2.2 \pm 0.4$	$0.038 \pm 0.004$	$42 \pm 4$	$0.290 \pm 0.013$	0.328	$16 \pm 1$
AnxA2 LUV L/P=150	$1.4 \pm 0.1$	$0.041 \pm 0.008$	$37 \pm 1$	$0.292 \pm 0.007$	0.333	$15 \pm 1$

<sup>a</sup> The semi-angle of the wobbling-in-cone subnanosecond motion was calculated as  $\omega_{max} = \arccos\{1/2[(1+8(\sum\beta_\omega/A_0)^{1/2})^{1/2}-1]\}$ , with  $\beta_\omega = \sum\beta_i$  (with associated  $\theta_i > 1$  ns); The intrinsic anisotropy  $A_0 = 0.370$  measured in vitrified medium was used (42). AnxA2<sup>acryl</sup> concentration: 0.5  $\mu$ M.

## FIGURE LEGENDS

Fig. 1. Fluorescence spectra of acrylodan in AnxA2<sup>acryl</sup>. Spectrum from 0.5  $\mu$ M protein in solution at pH 4 shows a maximum peak at about 515 nm (plain line). A blue shift is observed (peak at 470 nm) in the presence of phospholipid membranes (dotted line). The lipid protein molar ratio L/P is 100.

Fig. 2. Time-resolved fluorescence intensity decay and lifetime distribution of AnxA2<sup>acryl</sup>. A) Time-resolved fluorescence decay. Instrumental response function (curve 1); experimental decays of: AnxA2<sup>acryl</sup> at pH 4 in solution (curve 2); AnxA2<sup>acryl</sup> bound to LUV (PC/PS 75/25) L/P = 100 at pH 4 (curve 3). Experimental conditions are shown in the legend of Table 1. B,C) MEM reconstructed excited state lifetime distribution of AnxA2<sup>acryl</sup> at pH 4. B) AnxA2<sup>acryl</sup> in solution. C) AnxA2<sup>acryl</sup> associated to LUV (PC/PS 75/25) L/P = 100. Numerical values are shown in Table 1.

Fig. 3. Experimental fluorescence anisotropy decay of AnxA2<sup>acryl</sup> at pH 4. AnxA2<sup>acryl</sup> (curve A), AnxA2<sup>acryl</sup> bound to LUV (PC/PS 75/25) (L/P = 100) (curve B). Experimental conditions as in Table 1.

Fig. 4. Quenching of AnxA2<sup>acryl</sup> by doxyl PCs. Acrylodan fluorescence intensity was measured with LUV with different mole ratios of PC labelled with the quencher doxyl, at carbon positions 5 ( $\circ$ ) and 12 ( $\bullet$ ) of the acyl chain, as described in the methods section.

Fig. 5. Fluorescence emission spectra of AnxA2<sup>pyr</sup> at pH 4. 0.5  $\mu$ M protein in buffer (plain line). 0.5  $\mu$ M protein bound to LUV (PC/PS 75/25) L/P = 100 (dotted line). Excitation wavelength: 350 nm. Spectra normalized at 378 nm emission.

Fig. 6. Annexin 2-mediated membrane aggregation. A) LUV aggregation measured by turbidimetry at pH 4 ( $\bullet$ ) and at pH 7 with calcium (1 mM) ( $\circ$ ) as a function of AnxA2 concentration. B) Protein concentration dependent LUV aggregation at pH 4 for AnxA2 ( $\bullet$ ) and  $\Delta$ N-AnxA2 ( $\square$ ). Means of three independent experiments.

Fig. 7. Models for Annexin 2 membrane bridging. Schematic representation of the model for monomeric AnxA2 in membrane bridges. Two modes of organization of the protein are proposed: the classical calcium-dependent (A on the left) and the proton-dependent mechanisms (B on the right). Both modes are in equilibrium and the mode of organization of the membrane bridge is determined mainly by the balance in  $H^+$  and  $Ca^{2+}$  concentrations.  $Ca^{2+}$  favours the organization at the left and  $H^+$  favours the organization at the right. See text for details.

Figure 1

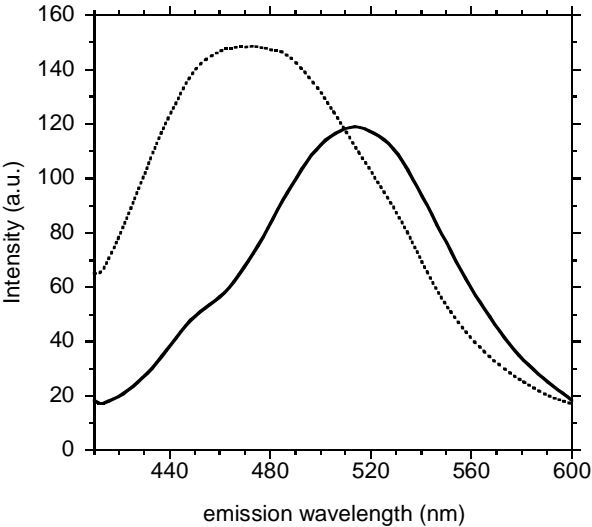


Figure 2

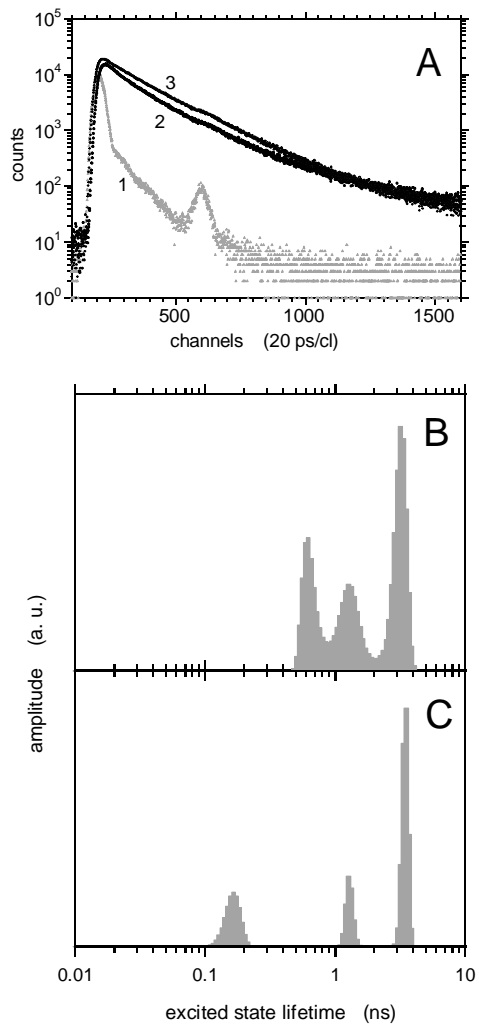


Figure 3

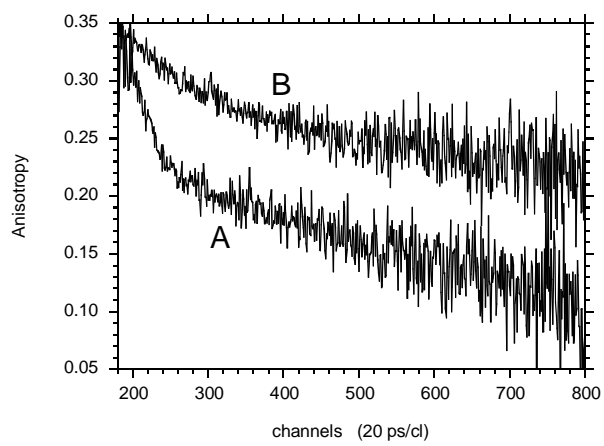


Figure 4

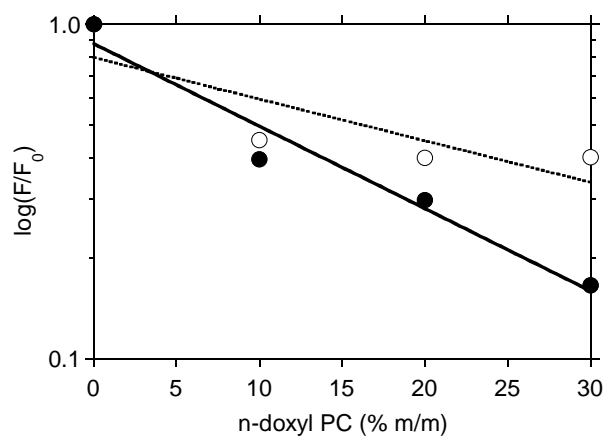


Figure 5

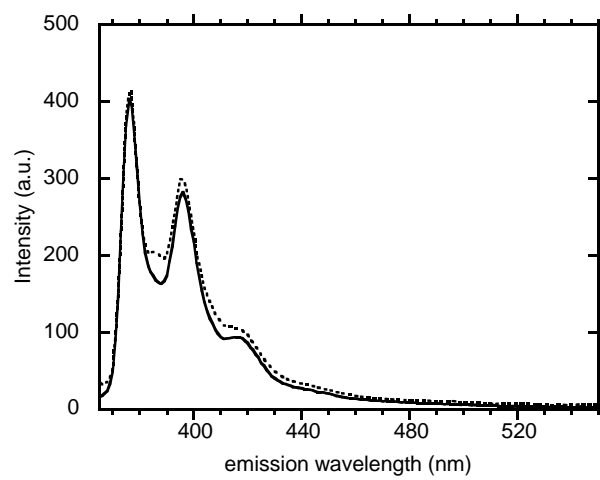


Figure 6

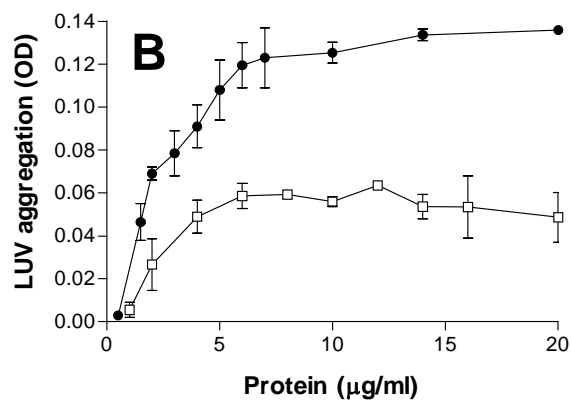
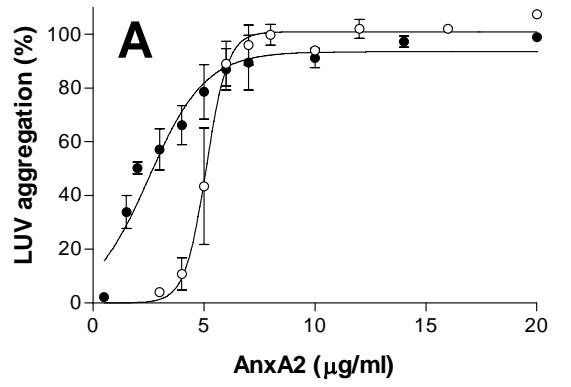


Figure 7

